Propagation Medium Impact on Sonar Coherent Processing for High Frequency Synthetic Aperture Imaging

Charles M. Ciany
Raytheon Company
Portsmouth, R.I. 02871 USA

Dr. George M. Walsh
Raytheon Company
Portsmouth, R.I. 02871 USA

Andrew M. Clark
Harbor Branch Oceanographic Institution
Ft. Pierce, Fl. 34946 USA

Abstract- Current capabilities of sidescan sonars to provide high resolution imaging at high area search coverage rates for today's minehunting and ocean bottom mapping applications are limited by the finite aperture lengths associated with practical physical constraints on the underwater vehicle. Synthetic aperture techniques hold the key to extending resolution beyond these limits, due to their ability to achieve the larger apertures through coherent combination of spatially sampled signals, generated using shorter apertures. In principle, the limiting resolution associated with these techniques is the spatial and temporal coherence of the medium over the combinations of design parameters required to achieve the desired imaging resolution at maximum range. Characterization of the underwater propagation medium's spatio-temporal coherence limitations is therefore a pre-requisite to an effective synthetic aperture sonar (SAS) system design.

Raytheon Company, in conjunction with Harbor Branch Oceanographic Institute, has designed and successfully conducted an acoustic medium stability experiment to provide such measurements. The experiment accurately characterizes the medium's coherence simultaneously in both space and time by employing a stationary acoustic projector and a large, stationary acoustic array that is long enough to encompass candidate SAS design lengths without requiring platform motion. Environmental and optical motion sensors are distributed along the array to monitor instantaneous physical changes, for removal of measurement variations that are not due to the medium. Conducted in October 1992 about 4 miles off the inlet to Port Everglades, Florida, the experiment measured the signal coherence in the 100 kHz to 300 kHz frequency band associated with potential SAS designs that could achieve a 2" resolution at 1000 ft range. Over sixty hours of data was collected, spanning a wide range of environmental conditions. The experiment is described, and the temporal coherence measurements are presented in terms of the probability distributions for amplitude and phase fluctuations over integration times representative of those required to form the high resolution SAS images. The results are then related to the SAS system design requirements.

I. Introduction

The major benefit of using Synthetic Aperture Sonar (SAS) in underwater imaging applications is the provision of near-optical quality imaging at practical area coverage rates without the need for large physical aperture sizes that carry with them impractical size, weight and power requirements for the host platform. Synthetic aperture techniques have been widely used in radar systems ([1], [2] and [3]), but only in recent years have they become practical for use in sonar. The SAS system forms the equivalent aperture sizes by employing coherent phase combination of the instantaneous pulsed sonar echo returns received from significantly smaller sampling apertures which are uniformly moved along the full

0-7803-1808-0/94 $4.00

path of the received aperture. Such an approach is well-suited to the use of Autonomous Underwater Vehicles (AUVs) for the host platforms. The key driving requirements for the system become 1) the amplitude and phase coherence required in the received signal over the coherent integration time used to form the equivalent aperture, 2) the associated inertial navigation accuracy required to limit image distortion arising from cross-track acceleration, and 3) the number of simultaneous received spatial beams needed to eliminate range ambiguity associated with the multiple resolution cells over which the AUV traverses during the two-way acoustic propagation time out to the maximum range. The major objective of the medium stability experiment was to determine and characterize the contribution of the underwater propagation medium to the received signal amplitude and phase fluctuations over the 100 kHz to 300 kHz frequency range which, when compared to the above requirements, would indicate the environmental conditions under which sufficient signal coherence is achieved to provide a 2-inch resolution at 1000 ft range without the use of post-processing compensation algorithms.

The azimuthal (i.e., along-track) imaging resolution requirements for the SAS system can be expressed in terms of the ratio of the length of the synthesized aperture, L_S, to the maximum slant range, R_0. Including the effects of beam broadening due to aperture shading, this ratio can be approximated by:

$$L_S / R_0 \approx 0.65\ c / (\delta x\ f_0) \qquad (1)$$

where δx = Azimuthal resolution (ft)
f_0 = Transmitted signal center frequency (Hz)
c = Average speed of sound (ft/sec)

Fig. 1 shows a plot of the required ratio as a function of frequency to provide the 2-inch resolution at a sound speed of 4990 ft/sec, which is characteristic of shallow water operating areas. From the figure, the synthetic aperture lengths at a maximum slant range of R_0 = 1000 ft are L_S = 194.6 ft and 64.9 ft. at the extremal test frequencies of 100 kHz and 300 kHz, respectively. The corresponding bounds on the received amplitude and phase fluctuations are obtained by using the results of Steinberg [4] to predict their effect on the ratio of the peak sidelobe level to the mainlobe level of the focused synthetic aperture beam. It is necessary to maintain a ceiling on this ratio, in order to insure sufficient contrast ratio in the coherently formed image for detecting objects of interest at the design resolution. Based on Steinberg's work, the probability distribution for this ratio can be approximated by:

$$\gamma \approx (\sigma_A^2 + \sigma_\phi^2)\,[1 + g(p) + 2/g(p)] / N_E \qquad (2)$$

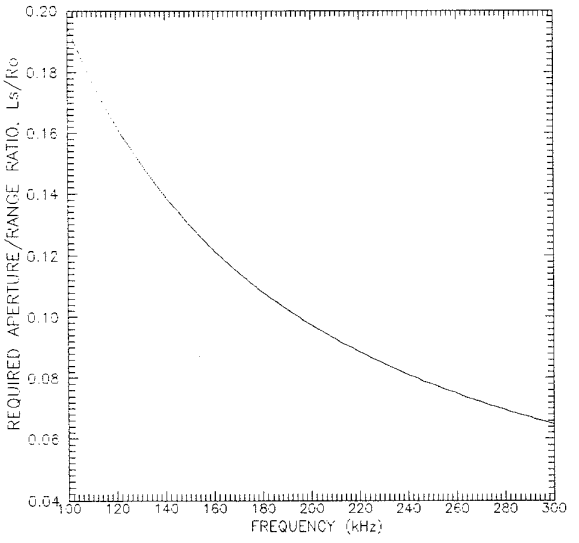

Fig. 1. Required Synthetic Aperture/Range Ratio vs. Frequency for 2-inch Image Resolution at 4990 ft/sec Sound Speed.

where p = Probability that the ratio of the peak sidelobe level to mainlobe level is less than γ
σ_A = RMS amplitude fluctuation (unitless)
σ_ϕ = RMS phase fluctuation (radians)
N_E = Equivalent number of sensor elements in the synthesized array,

and the function g() is given by:

$$g(p) = -ln(1 - p^{1/n}) \qquad (3)$$

The factor, n, in (3) is dependent on the geometry and pointing direction of the array. For a strip-mapping synthetic aperture array of length L_S in which the beams are steered in the direction perpendicular to the array, the array factor, n, and the equivalent number of elements, N_E, are given by:

$$n = (\lambda / L_S) \qquad (4)$$

$$N_E = 0.5\ L_S / \delta x \qquad (5)$$

where λ is the signal wavelength in ft.

Substituting (3) through (5) into (2) yields the resulting bounds on the amplitude and phase fluctuations. These bounds are plotted as a function of the 90th percentile peak sidelobe level (p = 0.9) in Fig. 2 for the various test frequencies at the maximum slant range of 1000 ft, using the aperture-to-slant range ratios of Fig. 1 and assuming equal amplitude and phase fluctuations (i.e., $\sigma_a^2 = \sigma_\phi^2 = \sigma^2/2$). Note that the required rms amplitude and phase fluctuations

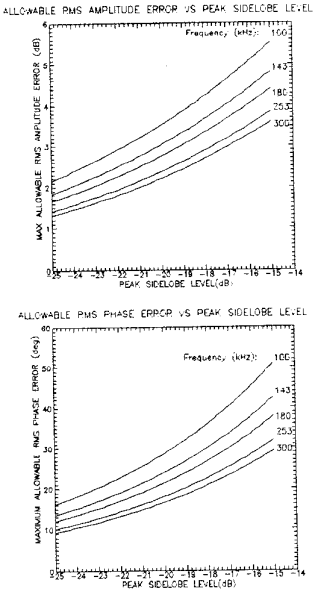

Fig. 2 Amplitude & Phase Error Budgets vs. Peak Sidelobe Level.

which limit the peak sidelobe-to-mainlobe ratio to -18 dB (deemed sufficient for high resolution imaging) go from 4.2 dB and 35 degrees at 100 kHz to 2.5 dB and 18 degrees at 300 kHz. The experiment was designed to accurately measure and resolve amplitude and phase fluctuations of these magnitudes.

II. Experiment Description

A. Site Selection

The medium stability experiment was conducted off the coast of Port Everglades, Florida. This site was chosen because 1) a 600 ft bottom depth is reached only 4 nautical miles off the coast, allowing operations crews to come ashore between daily operations, 2) its proximity to the Gulf Stream insured a wide range of environmental conditions, especially with regards to the ambient underwater currents, and 3) a coastal ranging station operated by the Naval Ship Warfare Center was available to provide an existing underwater cable for power and logistics support in positioning the array and projector.

B. Mechanical Design and Construction

The major mechanical components of the experiment were a billboard-style array structure and a tripod acoustic projector. The billboard is depicted in the photo of Fig.3, which was taken during its actual deployment at the test site. Constructed primarily of aluminum, it houses the following

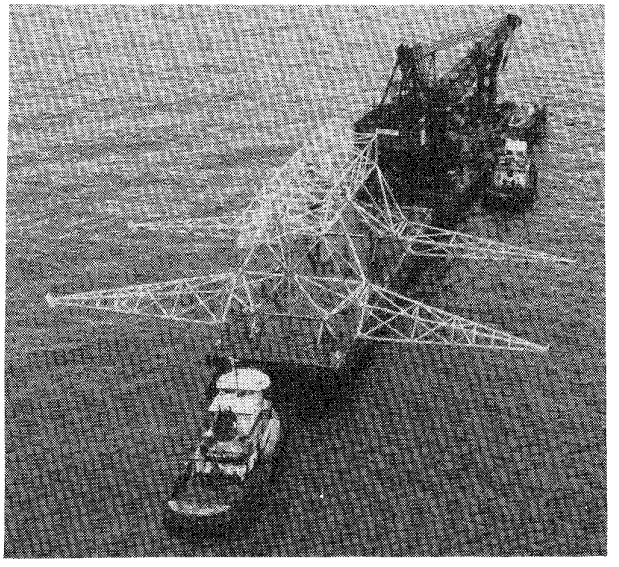

Fig. 3. Receiver Billboard Array During Test Deployment.

sensors: 1) a linear array of 10 non-uniformly spaced acoustic hydrophones, 2) a set of 4 environmental ("CTD") sensors which are sampled at a 19 Hz rate to produce time-varying temperature, conductivity, and pressure measurements for subsequent conversion to sound velocity and acoustic absorption loss estimates, 3) a suite of 12 strain gauges to measure the axial tension at various stress points on the billboard, 4) a set of 6 optical detectors (termed "laser targets") and their associate motor micrometers for measuring the transverse deflection of each hydrophone (i.e., in a direction perpendicular to the axis joining the hydrophones), and 5) auxiliary leak detectors and temperature sensors for fault detection.

The tripod projector, illustrated in Fig. 4, consists of two acoustic sources (one for redundancy) and a pan & tilt mechanism that is digitally controlled from the shore station to point the selected acoustic source at the center of the receiver array. The sources are designed to provide a minimum source level of 190 dB re 1 μPa over the test frequency band, at beamwidths wide enough to illuminate the full receiver array at test ranges of 500 ft or greater. The transmit sources and receive hydrophones are mounted at respective heights of 10 ft and 75 ft, which were determined to provide a minimum time delay of 300 μs from the start of each received direct-path acoustic pulse to that of the first bottom-bounce path. This time delay insures that the first 25 digital samples of each received pulse (the minimum number of samples required to accurately estimate signal amplitude and phase) are free of bottom-bounce multipath.

C. Hardware Design

The interconnection of the major hardware components is

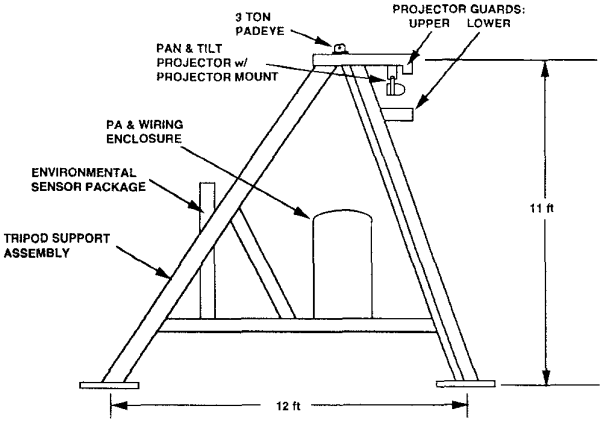

Fig. 4. Transmit Projector Tripod for Medium Stability Experiment.

illustrated in Fig. 5. The assemblies include the billboard array receiver electronics, the transmitter tripod electronics, and the shore station hardware. The shore station contains a PC/AT that is bridged to a VME chassis to control the transmission of pulsed CW transmission signals to the acoustic projector and the collection of digitized data from the various sensors. The acoustic transmissions ("pings") are sent at a 0.5 Hz rate. Four waveform generators are employed in the transmitter, providing the capability to simultaneously transmit dual CW frequencies and bandshift each frequency at each hydrophone output to a common 25 kHz baseband frequency. This processing results in a total of 20 channels of acoustic signals, two for each of the ten hydrophones. These signals are filtered to a 10 kHz bandwidth, digitized to 12 bits at an 83.33 kHz sample rate, multiplexed with the digitized environmental and mechanical sensor data, and stored in files in the PC/AT. The files are then copied onto magnetic tape for storage and post processing.

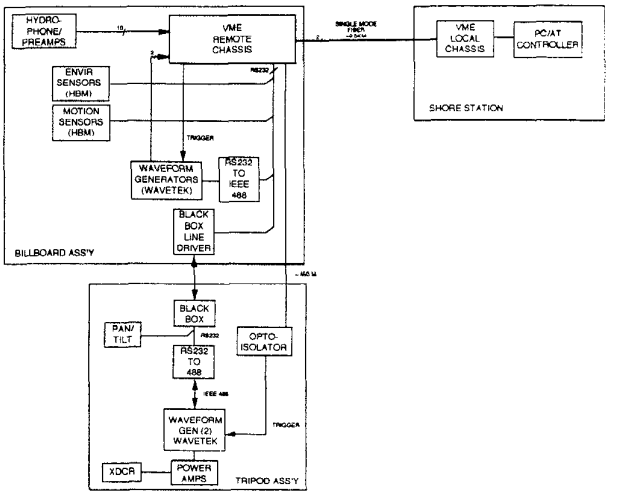

Fig. 5. Overall Hardware Diagram for Medium Stability Experiment.

D. Receiver Signal Processing

The data analysis processing flow shown in Fig. 6 consists of the following five major processing functions.

1) *Environmental Processing:* The local sound velocity at the receive array and the absorption over each transmitter-to-hydrophone direct acoustic path are estimated from the Conductivity/Temperature/Depth (CTD) sensors mounted on the array, using the models in [5] and [6], respectively. The estimates are then low pass filtered to a 5 Hz bandwidth.

2) *Mechanical Processing:* The transverse hydrophone deflections along the receiver array are measured using the sampled motion data from the laser targets and strain gauges.

3) *Single-Ping Acoustic Processing:* The received signal amplitude and phase are estimated for each of the 20 baseband acoustic channels on each ping.

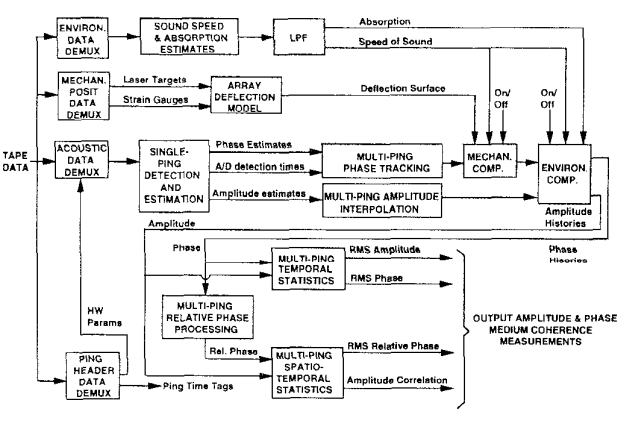

Fig. 6. Data Analysis Processing Block Diagram.

4) *Multi-Ping Acoustic Processing:* The single-ping amplitude and phase estimates are tracked from ping-to-ping to generate time series "histories." Optional compensation is performed using the environmental and mechanical estimates to remove any significant measured fluctuations that are not due to the medium. The compensated phase histories are processed relative to the middle hydrophone of the receive array to derive the geometry-removed residual phase fluctuations.

5) *Multi-Ping Statistics Processing:* "Temporal-only" amplitude and phase statistics are computed from the corresponding multi-ping histories of each hydrophone, and "spatio-temporal" phase statistics are calculated from the multi-ping, multi-hydrophone relative phase histories.

III. Results

The acoustic medium stability experiment commenced on 12 October, 1992, after the receiver array and transmitter tripod segments were successfully deployed at depths of 576 ft and 546 ft, respectively, with a measured direct-path separation of 990 ft. By processing the differential time delays to the end hydrophones of the array, the azimuthal alignment of the tripod was measured to be 8.6 degrees from the perpendicular bisector to the array, as shown in the deployment summary of Fig. 7. The pan & tilt mechanism on the tripod was remotely adjusted from the shore station to maximize the received signal-to-noise ratio at the center of the array, and data was then collected over the ensuing 5-week period. Over 65 hours of data were archived to tape, with specific frequency and pulsewidth combinations as shown in Table I. Approximately 20% of this data has been processed to date. Received Signal-to-Noise Ratio (SNR) was generally well in excess of 20 dB over the test frequency range, with corresponding pulse leading edges free of any interfering bottom or surface bounce multipath. The multi-ping statistics were generated on 15-minute data segments, producing coherence measurements in terms of probability distributions for amplitude and phase fluctuations over integration times representative of those required to form the SAS images at a constant AUV platform speed of 5 knots. The experimental results are summarized in the remaining sections.

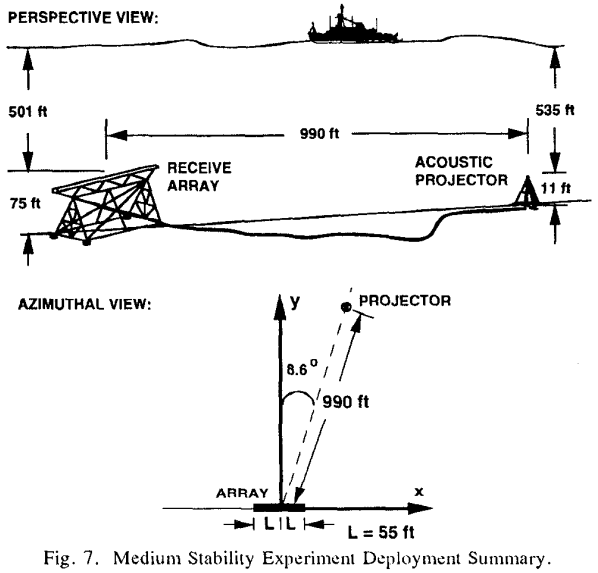

Fig. 7. Medium Stability Experiment Deployment Summary.

TABLE I
SUMMARY OF EXPERIMENTAL DATA COLLECTED

Frequency (kHz)	Pulsewidth (ms)	Total Data Collected (min)
100	0.30	20
100	0.75	36
100	1.50	1867
143	1.50	464
180	0.75	28
180	1.50	204
253	0.75	27
253	1.50	859
300	0.75	29
300	1.50	391
TOTAL DATA COLLECTED:		3925 min

A. Environmental Conditions

Data was collected at varying times of day, spanning a diversity of surface weather conditions that ranged from calm to tropical depression winds of up to 40 knots. The processed environmental data indicated a wide range of ambient current conditions, ranging from near zero current to 3/4 knots. During a portion of the data collection, a separate crew operated in the vicinity of the array, dropping Conductivity/Temperature/Depth (CTD) sensors from the surface to the bottom, to obtain vertical profiles of the sound velocity. Fig. 8 shows the associated extremal profiles that were computed from these measurements, indicating significant variability over the time frame of the experiment.

B. Mechanical Stability

The mechanical data indicated that the array was very stable, and thus there was no need for mechanical compensation of the data in the post-processing. For example, Fig. 9 shows the laser target deflection measurements at the beginning and near the end of the experiment, indicating an upper bound of

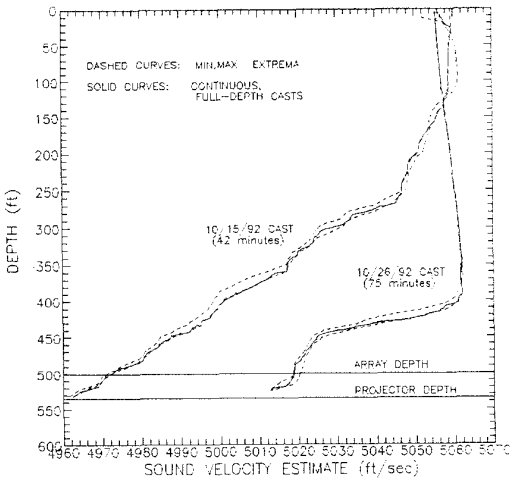

Fig. 8. Sound Velocity Profiles Generated From Processed Oceanographic Data.

about 4 mils, which translates to less than 8 degrees of signal phase fluctuation at the 300 kHz test frequency.

C. Environmental Compensation

Environmental compensation to amplitude and phase was attempted using the local sound speed and absorption estimates generated from the CTD sensors mounted on the array. Although the trends in the phase excursion over a 15-minute processing segment correlated with those of the measured local sound speed at the array, the short-term ping-to-ping phase fluctuations were uncorrelated with those of the local sound speed. Apparently, local estimates made at the receiving array do not track the actual sound speed over the full acoustic path lengths from the projector to the array. Local sound speed compensation is thus deemed ineffective at reducing fluctuations due to the medium.

D. Array Performance Predictions

The temporal amplitude and phase fluctuations from the processed single-hydrophone data were generally within the required bounds for imaging over a majority of the time at the lower test frequencies. For example, Fig. 10 shows a plot of the distribution of rms amplitude and phase at the extremal test frequencies for "moderate" ambient current levels of about 1/3 knot. Note that the rms phase variability at the 75th percentile level goes from 35 deg at 100 kHz to 55 deg at 300 kHz, while the corresponding amplitude variations go from 1.4 dB to 2.2 dB.

The magnitude of the temporal amplitude and phase fluctuations also exhibited strong correlation to that of the ambient underwater ocean currents, as illustrated in the single-hydrophone data of Fig. 11. The measured distributions of rms amplitude and phase at 100 kHz show increasing fluctuation with increasing ocean current.

The synthetic aperture array performance can also be predicted by substituting the measured amplitude and phase distributions directly into the peak sidelobe level expression of (2). For example, Fig. 12 shows the predicted peak

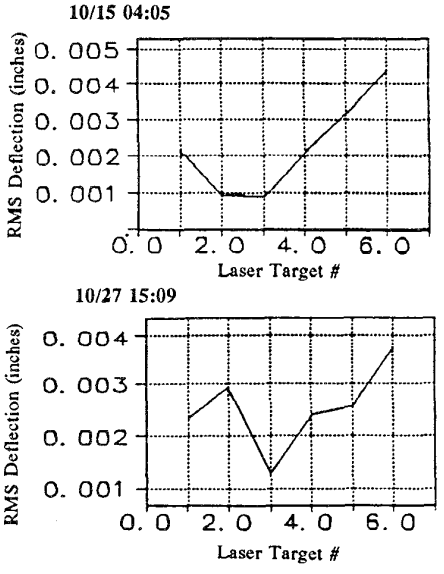

Fig. 9. Sample Mechanical Data Showing Array Stability.

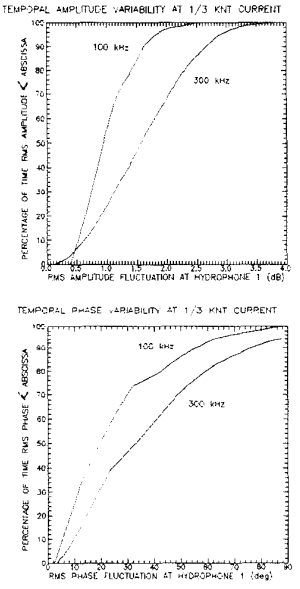

Fig. 10. Variation of Amplitude & Phase Fluctuations with Frequency.

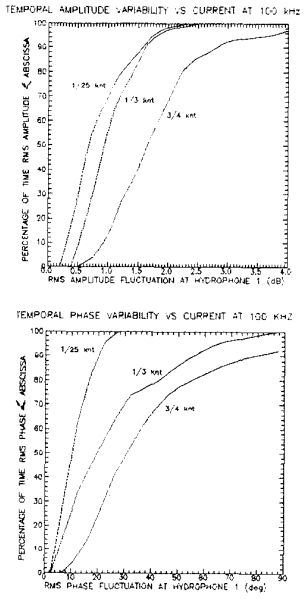

Fig. 11. Variation of Amplitude & Phase Fluctuations with Ambient Ocean Current.

sidelobe levels for the 100 kHz and 300 kHz data of the previous two figures.

The multi-sensor processing results indicate that the spatio-temporal fluctuations are within bounds under the following very limited condition: near-zero currents, or currents which were "steady-state" in their strength and direction. This is most dramatically illustrated in the "phasor" representation [7] of the processed data, in which

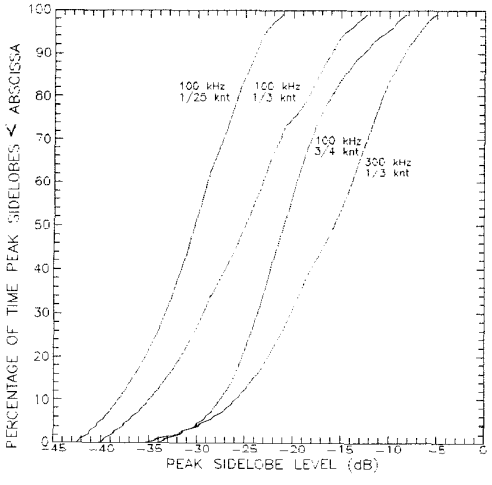

Fig. 12. Distributions of Peak Sidelobe Level Derived From Measured Temporal Amplitude & Phase Fluctuations.

the multi-ping estimates are plotted as a rotating vector whose instantaneous radius is equal to the measured amplitude and whose instantaneous angle is equal to the measured phase.

Fig. 13 shows a phasor plot of the 100 kHz and 253 kHz data from the first and last days of data collection. Note the significant improvement in medium coherence on the last day, indicated by the appearance of circular arcs. The corresponding interpretation is that the amplitude variations are small (exhibited by the narrow width of the arc), and the phase variations are slow (since the data segments from one ping to the next "travel" along the arc). Note that the phase wander over each 15 minute test period on the last day is restricted to about 90 deg at 100 kHz and 180 deg at 253 kHz. Conversely, the data from the first day exhibits phase wander of greater than 360 degrees, with significantly greater fluctuations. The associated environmental conditions for the data of Fig. 13 indicated that the magnitude of the current was comparable (about 1/3 knot), but a key difference existed in the behavior of the current's direction. In the highly stable data from the last day of the data collection (the right half of the Fig. 13), the current was steady in its course, with a fluctuation of only 4 degrees. In contrast, the current on the first day shows a significantly larger fluctuation in its course of about 15 degrees. The associated peak sidelobe predictions from the relative phase distributions on the last day are shown in Fig. 14.

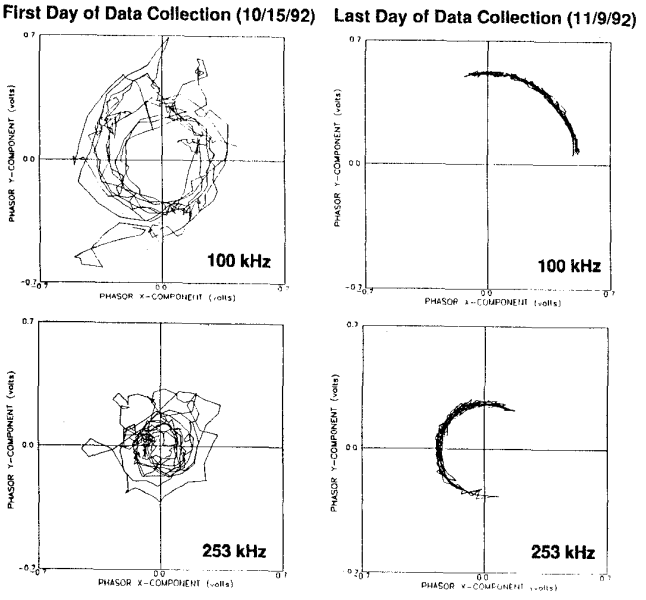

Fig. 13. Phasor Depiction of Medium Stability.

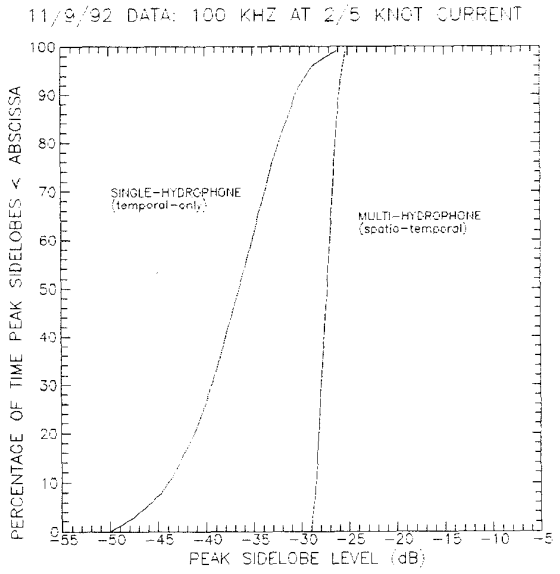

Fig. 14. Peak Sidelobe Distributions Derived From Measured Spatio-Temporal Amplitude & Phase Fluctuations of 11/9/92 Data.

IV. Conclusions

The above results show the strong influence of the underwater current on the acoustic medium stability. The amplitude and phase fluctuations are typically proportional to both the magnitude of the underwater current and its fluctuations in direction. While the processed single-hydrophone data showed that the temporal amplitude and phase fluctuations were within the bounds required for 2-inch imaging resolution at 1000 ft ranges over a majority of the time, the multi-hydrophone processing results show that when the spatial extent of the required synthetic aperture lengths is also taken into account, the medium only appears to support this imaging resolution under limited environmental conditions of steady-state ambient currents. For operation in shallow-water areas (of interest in minehunting applications), in which the underwater currents fluctuate due to the influence of underwater tides, some form of auto-focus processing will likely be required to compensate for medium distortions in order to meet the above operating resolution and area coverage with any high degree of system availability over the 100 kHz - 300 kHz frequency band which was tested. Note that, while the medium does not support the above design resolution and coverage without auto-focus techniques, it is possible to process the data from the medium stability experiment to determine the combination of reduced resolution and coverage rates which would be supported without the need for auto-focusing.

V. Acknowledgments

The authors wish to acknowledge the dedication and efforts of those engineers at Raytheon and Harbor Branch Oceanographic Institution who contributed to the medium stability experiment. In particular, M. Sherry provided invaluable coordination and management during hardware integration and actual testing; P. Koussa was steadfast in supporting test integration, hardware maintenance, and operation of shore based equipment at the test site; and S. Johnson and T. McHale provided key assistance in the data collection and evaluation.

V. References

[1] A.W. Rihaczek, "Principles of High-resolution Radar", New York, McGraw Hill, 1969.

[2] R.O. Harger, "Synthetic Aperture Radar Systems", New York, Academic Press, 1970.

[3] J.P. Fitch, "Synthetic Aperture Radar", New York, Springer-Verlag, 1988.

[4] B.D. Steinberg, "Principles of Aperture and Array Systems Design", John Wiley & Sons, 1976.

[5] R. J. Urick, "Principles of Underwater Sound", New York, McGraw-Hill, Inc., 1975, p.105.

[6] R. E. Francois and G. R. Garrison, "Sound Absorption Based on Ocean Measurements. Part II: Boric Acid Contribution and Equation for Total Absorption," J. Acoust. Soc. Am., Vol. 72, No. 6, December 1982.

[7] S. Flatte, "Wave Propagation Through Random Media," Proc. IEEE, Vol. 71, No. 11, Nov. 1983.